令和 2 年 5 月発行 Journal of Magnetic Resonance Imaging 誌
第 51 巻 第 5 号 1497 頁～1506 頁掲載

Evaluation of image quality of pituitary dynamic contrast-enhanced MRI using time-resolved angiography with interleaved stochastic trajectories (TWIST) and iterative reconstruction TWIST (IT-TWIST)

Yusuke YOKOTA[1], Yasutaka FUSHIMI[1]*, Tomohisa OKADA[2], Koji FUJIMOTO[2], Sonoko OSHIMA[1], Satoshi NAKAJIMA[1], Toshihito FUJII[3], Masahiro TANJI[4], Nobuya INAGAKI[3], Susumu MIYAMOTO[4], and Kaori TOGASHI[1]

[1]*Department of Diagnostic Imaging and Nuclear Medicine, Graduate School of Medicine, Kyoto University, Kyoto, Japan,*
[2]*Human Brain Research Center, Graduate School of Medicine, Kyoto University, Kyoto, Japan*
[3]*Department of Diabetes, Endocrinology and Nutrition, Graduate School of Medicine, Kyoto University, Kyoto, Japan,*
[4]*Department of Neurosurgery, Graduate School of Medicine, Kyoto University, Kyoto, Japan,*

Abstract

BACKGROUND: Time-resolved angiography with interleaved stochastic trajectories (TWIST) is a keyhole imaging with frequent sampling of central k-space data and view-sharing for the peripheral k-space of dynamic phases. IT-TWIST is a technique to reconstruct images with a smaller temporal footprint using the same raw data obtained with TWIST by iterative reconstruction.

PURPOSE: To compare image quality between TWIST and IT-TWIST in 3D pituitary DCE-MRI.

STUDY TYPE: Retrospective observation study.

POPULATION: 51 patients (23 men, 28 women) who underwent 3D pituitary DCE-MRI using TWIST between July 2016 and April 2017.

FIELD STRENGTH/SEQUENCE: 3T/TWIST and IT-TWIST.

ASSESSMENT: Visual evaluation was conducted for image quality of delineation of the pituitary stalk and posterior lobe during the early arterial phase, cerebral white matter near the sella turcica, and the mass lesion. Bolus sharpness of the pituitary stalk, posterior lobe, and bilateral cavernous sinus was evaluated on the enhancement slope map calculated from TWIST and IT-TWIST. Temporal stability of intensity of non-enhanced area was evaluated on temporal standard deviation (SD) map calculated from TWIST and

IT-TWIST.

STATISTICAL TESTS: Paired t-test or Wilcoxon rank-sum test was used to test the differences between TWIST and IT-TWIST in both visual evaluation and ROI evaluation.

RESULTS

Scores of visual evaluations for IT-TWIST were significantly better than those for TWIST (P <0.001) in all items. Enhancement slope for IT-TWIST was significantly higher than that for TWIST in posterior lobe, right and left cavernous sinus (P < 0.001). Temporal SD for IT-TWIST was significantly lower than that for TWIST in all items with statistical significance (P < 0.001).

DATA CONCLUSION: IT-TWIST yielded better visualization, and better enhancement slope, and less temporal SD compared with TWIST in 3D pituitary DCE-MRI.

Evidence Level 4: Observational retrospective case series.

Stage 1: Technical Efficacy

Key words

Magnetic Resonance Imaging； Pituitary Gland; Central Nervous System

Introduction

Pituitary dynamic-contrast enhanced (DCE) magnetic resonance imaging (MRI) is useful in visualizing the complex blood perfusion system of the pituitary gland. The pituitary stalk and posterior lobe are supplied by the superior, middle and inferior pituitary arteries arising from the intracranial portions of the internal carotid artery. The anterior lobe is mainly supplied by the hypothalamic-pituitary portal circulation to carry hypothalamic stimulatory and inhibitory hormones.[1,2] Due to such differences in blood supply, the posterior lobe and pituitary stalk are enhanced in the early arterial phase, and anterior lobe is enhanced later. Pituitary DCE-MRI visualizes details of the normal pituitary structures in the early arterial phase and the relationship between the pituitary and surrounding lesions, and the usefulness of pituitary DCE-MRI was reported in pituitary adenoma, including microadenomas and other diseases.[3-8] Identification of the normal pituitary gland compressed by macroadenoma is very important to preserve the normal pituitary gland during surgery.[9] If normal early enhancement of pituitary posterior gland is not detected, posterior lobe abnormalities such as lymphocytic hypophysitis and Langerhans cell histiocytosis may be suspected.[5]

Improving the temporal and spatial resolution and image quality of pituitary DCE-MRI is important to improve the understanding of dynamic enhancement

information for pituitary diseases. Two-dimensional acquisition (2D) was initially used in dynamic MRI,[3,4] and several works have reported the utility of three-dimensional (3D) pituitary DCE-MRI.[10,11] More advanced techniques have been applied for pituitary DCE-MRI, such as compressed sensing MR using golden-angle radial sparse parallel technique for identifying normal pituitary gland in patients with macroadenoma.[12,13] Time-resolved angiography with interleaved stochastic trajectories (TWIST) is another advanced technique, representing a keyhole imaging modality with frequent sampling of central k-space data and view-sharing for the peripheral k-space of dynamic phases.[14-17] High temporal and spatial resolutions can be achieved with TWIST by sharing several peripheral areas of k-space (region B) in neighboring dynamic phases, while the central area of k-space (region A) is acquired for each dynamic phase image. Currently, TWIST is also used for DCE of non-vascular organs such as breast and prostate.[18,19] Furthermore, iterative reconstruction of TWIST (IT-TWIST) has been introduced because of the shorter temporal footprint compared to TWIST (Fig. 1).[20] IT-TWIST is a technique to reconstruct images with a smaller temporal footprint using the same raw data obtained with TWIST by iterative reconstruction using a compressed sensing technique.[20] Application of IT-TWIST to non-vascular organs has not been reported. No reports have described the use of TWIST and IT-TWIST techniques for pituitary DCE-MRI. We hypothesized that

shorter and actual temporal footprint images with IT-TWIST were more useful in pituitary DCE-MRI, as previously reported for targeting vascular disorders.[20] The aim of this study was thus to compare image quality between TWIST and IT-TWIST in 3D pituitary DCE-MRI.

Materials and methods

Patients

This retrospective observational study was approved by the institutional review board and the need to obtain informed consent was waived. Inclusion criteria were as follows. Subjects comprised 51 consecutive patients (23 men, 28 women) who underwent pituitary DCE-MRI using TWIST between July 2016 and April 2017. These cases involved either clinical suspicion of sella or parasellar lesions or follow-up for postoperative observation of pituitary disease. The only exclusion criterion was excessive imaging artifact due to patient's movement during pituitary DCE-MRI. Mean age was 53.6 years (range, 9-83 years). Demographic details of disease are shown in Table 1.

MR imaging

The 3D pituitary DCE-MRI imaging was conducted on a clinical 3-T MR unit (MAGNETOM Skyra, Siemens Healthineers AG, Erlangen, Germany) using a 32-channel head coil. Contrast injection was performed with a 0.1-mmol/kg patient weight dose of gadolinium-based contrast media

and 20 mL of normal saline injected at a rate of 4 mL/s via the antecubital vein 10 s after starting the pituitary DCE-MRI scan.

TWIST and IT-TWIST imaging

TWIST improves the apparent temporal resolution using a unique k-space acquisition method. The k-space is divided into two parts as mentioned in the Introduction: a central part (region A); and a peripheral part (region B) (Fig. 1). Region A contributes to the overall contrast of the image and area, and region B contributes to the rendering of a fine structure. In TWIST, region A and one of the subsegments of region B (subregion B1-B4, in this case) are alternately acquired for each phase (Fig. 1). At that time, region A data is fully acquired and region B data are acquired sparsely. Images for each time frame are created from one specified region A and a collection of subsegments in region B of the neighboring other dynamic phases. On the other hand, in IT-TWIST, images for each time frame are retrospectively created from 1 region A and 1 subregion

in B of the same k-space data with TWIST by using an iterative reconstruction algorithm (Fig. 2). "Temporal resolution" is defined as the time needed to fill one trajectory in region A plus subregion B in k-space, and "temporal footprint" is the total time of the data used for image reconstruction (actual temporal resolution). In both TWIST and IT-TWIST, apparent temporal resolution used for image reconstruction is "the sum of acquisition times for 1 region A plus 1 subregion B". The temporal footprint is reflected in images as the sum of acquisition times for multiple region As and subregion Bs in TWIST, whereas the temporal footprint is identical with the specified temporal resolution for IT-TWIST (Fig. 1).

MR imaging parameters

Imaging parameters for TWIST DCE-MRI in this study were as follows: coronal acquisition; TR/TE, 2.84/1.10 ms; flip angle, 5°; matrix, 203 × 250; field of view, 203 × 250 mm; slice thickness, 1 mm, isotropic voxel, 1 mm; slice per slab, 52; phase partial Fourier, 7/8; slice partial Fourier, off; acceleration factor of 2 with GeneRalized Autocalibrating Partial Parallel Acquisition (GRAPPA); size of fully sampled central k-space region A, 20%; sampling density of peripheral k-space region B, 25%; acquisition time for each time frame, 6.17 s; and number of time frames, 15. TWIST images were

reconstructed with the online (product) reconstruction pipeline. Afterwards, iterative reconstruction based on prototype software was retrospectively performed on the scanner (using Modified Fast Iterative Shrinkage-Thresholding Algorithm (mFISTA) algorithm with the redundant Haar wavelet transform a k-t regularization factor of 0.002 and 20 iterations). [21] The temporal footprint of "3 region As and 4 subregion Bs" was 21.60 s in TWIST, and that of "1 region A and 1 subregion B" was 6.17 s in IT-TWIST. The retrospective reconstruction time for IT-TWIST was about 8 min employing the graphics processing unit of the reconstruction hardware. In addition, CE 3D T1 gradient echo sequence (volumetric interpolated breath-hold examination, VIBE) were obtained subsequently after TWIST DCE-MRI in our pituitary MR protocol. Imaging parameters of CE-VIBE were as follows: sagittal acquisition; TR/TE, 6/4.7 ms; flip angle, 15°; matrix, 320×320; field of view, 220×220 mm; slice thickness, 0.7 mm; slices per slab, 240.

Visual evaluation of TWIST and IT-TWIST DCE-MRI

Three board-certified neuroradiologists (Y.Y, 10 years of experience and S.O, 9 years of experience and S.N, 15 years of experience) independently evaluated image quality of TWIST and IT-TWIST in terms of delineation of posterior lobe, delineation of pituitary stalk during the early arterial phase, and image quality of cerebral white matter

near the sella turcica. When a mass lesion was observed, raters evaluated delineation of the mass lesion border compared to normal pituitary parenchyma. Patient information as well as sequence names and series numbers were anonymized. All images were presented in 4D multi-planar view using AQnet (TeraRecon, Foster City, CA). Window width and window level were prescribed and the same values were used for the same cases of TWIST and IT-TWIST images. To evaluate image quality of delineation of posterior lobe and pituitary stalk, reference images for 5-grade scoring systems were made from a CE 3D T1 gradient echo sequence (volumetric interpolated breath-hold examination, VIBE) subsequently obtained after post-dynamic images from one of the patient datasets (grade 5 was best). Imaging parameters of CE-VIBE and details of 5-grade scoring systems were shown in Fig. 3. In cases where enhancement of the posterior lobe or pituitary stalk was difficult to recognize, the examination was excluded from evaluation of the posterior lobe or pituitary stalk. Interrater reliability was calculated, and final evaluations were made on the consensus decision of raters.

Region of interest (ROI) evaluation

We quantitatively evaluated TWIST and IT-TWIST images for bolus sharpness and stability of intensity in DCE among each dynamic phase. We inspected all images

and found no head motion. Parametric images of TWIST and IT-TWIST were calculated from 15 phases of dynamic images using Matlab 2014 (The MathWorks Inc., Natick, MA). The details of pixel-by-pixel parametric images were as follows. i) enhancement slope was defined as the linear slope passing through the points of 20% and 80% between minimal and maximum signal intensity on the curve-fitted time intensity curve (TIC), thus creating an enhancement slope map (Fig. 2). ii) Temporal standard deviation (SD) maps were created by calculating standard deviation of 15 dynamic-phase images (Fig. 2). The enhancement slope and temporal SD were regarded as indexes of DCE bolus sharpness and indicators of the temporal stability of intensity for the non-enhanced area among each dynamic phase.

One board certified neuroradiologist (Y.Y, 10 years of experience) placed 2-mm × 2-mm ROIs in the posterior lobe, pituitary stalk, bilateral cavernous sinus, sinus air, parasellar cerebrospinal fluid (CSF), ventricular CSF, and corpus callosum with reference to coronal plane images using ImageJ software (https://imagej.nih.gov/ij). ROIs were carefully placed without including boundaries to avoid partial volume effects. Posterior lobe was defined as the pituitary posterior area showing high intensity in the first dynamic phase (non-enhanced phase) or enhanced area in the early arterial phase around the 4th dynamic phase which corresponded to 21.4 s from injection.[22] ROIs of posterior lobe,

pituitary stalk, and bilateral cavernous sinus were applied to enhancement slope map image. ROIs of sinus air, parasellar CSF, ventricular CSF and corpus callosum were applied to temporal SD map images. Two board certified neuroradiologists (S.O, 9 years of experience, Y.F, 20 years of experience) approved all ROI placements.

Statistical analysis

For evaluations of visual quality, Wilcoxon rank-sum test was used to compare TWIST and IT-TWIST. Interrater reliability was calculated with intraclass correlation (ICC) (two-way mixed, average measures, absolute agreement). In ROI analyses, paired t-tests were used for comparing TWIST and IT-TWIST. If the data did not display a normal distribution by Shapiro-Wilk test, Wilcoxon rank-sum test was used. Because these analyses were applied multiple times, Bonferroni correction was used in both visual evaluations and ROI analyses, independently. All tests were two-sided and values of $P < 0.05$ were defined as statistically significant. When Bonferroni correction was used to adjust for multiple comparisons, values of $P < 0.0125$ (0.05/4) in visual evaluations of 4 areas and $P < 0.00625$ (0.05/8) in ROI evaluations of 8 regions were defined as statistically significant. Statistical analysis was performed using MedCalc version 18 software (MedCalc Software bvba, Ostend, Belgium).

Results

Visual evaluation

We visually evaluated posterior lobes (n = 44), pituitary stalks (n = 46), white matter (n = 51). In the other cases out of total 51 cases, visual evaluation was difficult due to tumor compression. In addition, total 25 mass lesions were visually evaluated, they consisted of macroadenoma (n = 19), microadenoma (n = 3) and Rathke's cleft cyst (n = 3). Scores of visual evaluations for TWIST and IT-TWIST were shown in Fig 4. Scores of IT-TWIST were better than those of TWIST with statistical significance (P <0.001) in all items. ICC values were posterior lobe, 0.76; pituitary stalk, 0.76; white matter, 0.73; and mass lesion, 0.70.

ROI evaluation

We performed ROI evaluation of enhancement slope in posterior lobe (n = 44), pituitary stalk (n = 45), right cavernous sinus (n = 46), and left cavernous sinus (n = 49). In the other cases out of total 51 cases, ROI evaluation was difficult due to tumor compression. Enhancement slope for IT-TWIST was higher than TWIST in all items and statistical significance (P < 0.001) was seen in posterior lobe, right and left cavernous

sinus (Table 2, Fig. 5a).

We performed ROI evaluation of temporal SD in all patients (n = 51). Temporal SD for IT-TWIST was lower than that for TWIST in all items with statistical significance ($P < 0.001$) (Table 3, Fig. 5b).

Representative TWIST and IT-TWIST images with normal pituitary, microadenoma, and macroadenoma are shown in Fig. 6, 7 and 8. Early enhancement of pituitary stalk and posterior lobe are better visualized in IT-TWIST than TWIST. IT-TWIST shows less noise in parasellar CSF and sinus air, corpus callosum and ventricular CSF compared with TWIST.

Discussion

In visual assessments, IT-TWIST scored higher than TWIST in all items in this study. High-resolution 3D pituitary DCE-MRI remains challenging, and image quality is not fully guaranteed, therefore, IT-TWIST may add values in the dynamic evaluation of pituitary lesions. In addition, even where pituitary structures were deformed due to macroadenoma, we succeeded in identifying the pituitary stalk and posterior lobe by referring to arterial-phase images with both TWIST and IT-TWIST. In the diagnosis of diabetes insipidus, evaluation of signal intensity of posterior lobe and enhancement is

important, however, the identification of posterior lobe is sometimes difficult when signal intensity on T1-weighted image is low or intermediate. Better identification of enhancement of posterior lobe help radiologists evaluate the posterior lobe on precontrast T1-weighted image. Better visualization of posterior lobe enhancement is also valuable in differentiation of normal posterior lobe from other hyperintense lesions such as hemorrhage, degeneration and Rathke's cleft cyst.[23,24] Early enhancement of pituitary stalk is also useful to evaluate the normal pituitary gland severely compressed by pituitary or parasellar tumors. Our time-resolved 4D image sets enabled use of a multi-planar view method. Multiple dynamic phases were easily evaluated in axial, coronal, and sagittal views simultaneously in cine mode, which was readily applied in clinical practice.

Enhancement slopes of posterior lobe and bilateral cavernous sinus were higher in IT-TWIST compared with TWIST. Arterial blood is known to rapidly flow into the cavernous sinus,[25] and higher enhancement slope of cavernous sinus as well as posterior lobe in IT-TWIST represents higher bolus sharpness and higher contrast changes among the dynamic phases due to the shorter temporal footprint of IT-TWIST. Laterality of enhancement pattern in cavernous sinus may reflect the differences of venous drainage in cavernous sinus. Laterality of enhancement pattern may be associated with carotid cavernous sinus, infectious and inflammatory cavernous lesions,[26] therefore, DCE-MRI

based on the actual temporal resolution may provide clinical impacts in evaluation of cavernous sinus diseases. Our results are consistent with a previous study of thoracic blood vessels.[20] When the temporal footprint is longer, the time range reflected in the signal will be likewise longer, and temporal blurring will occur.[20,27] Shorter temporal footprint is attributable to the higher stability of the signal in IT-TWIST compared to TWIST especially in enhanced regions such as posterior lobe, pituitary stalk, cavernous sinus and mass lesion. Enhancement slope of the pituitary stalk in IT-TWIST was higher than that with TWIST, however, the difference was not statistically significant. IT-TWIST contributes to the signal stability reflecting actual temporal resolution, however, accurate signal in pituitary DCE-MRI and the values of enhancement slope may be different issues. The partial volume effect of CSF in ROIs of the pituitary stalk may have affected the results, because the pituitary stalk was the smallest structure in the ROI analyses conducted in this study.

Temporal SD in parasellar CSF, ventricular CSF, sinus air, and corpus callosum was significantly lower in IT-TWIST than that TWIST. Denoising of iterative reconstruction may be attributable to the higher stability of the signal in IT-TWIST compared with TWIST, especially in less enhanced regions such as cerebral white matter, parasellar CSF, ventricular CSF, sinus air and corpus callosum. Reduced temporal SD is

important in observations using a 4D multi-planar view. Although a trade-off exists between temporal footprint and image quality, IT-TWIST improved both compared with TWIST according to the results from both visual evaluations and ROI analyses in this study.

As features of this study, first, although the usefulness of IT-TWIST has been reported in MR angiography, no previous studies appear to have described results for non-vascular organs. Compressed sensing reconstruction technique can also be useful for DCE of other parenchymal organs. Second, comparing two different DCE image sequences for patients is difficult, because injecting gadolinium-based contrast media twice is not clinically reasonable given the risks of nephrotoxicity. Previous studies have conducted DCE comparisons using reconstructions from TWIST, and we therefore performed quantitative and qualitative evaluations in accordance with those methods.[20,27] Third, normal structures and mass lesions were appropriately detectable in visual evaluation in TWIST as well as IT-TWIST.

Our study had several limitations. First, we did not evaluate the diagnostic value for detecting microadenoma in this study. Although with the limited number of preoperative microadenoma, IT-TWIST yielded better visualization of microadenoma in all preoperative cases. Further investigation is necessary for demonstration of clinical

value of 3D pituitary DCE-MRI with IT-TWIST. Second, no motion correction was applied for 3D pituitary DCE-MRI in this study as previous reports.[12,13] However, it was confirmed that there was no visually obvious head motion, and no error was detected in this analysis. Third, our study used a retrospective design. Fourth, our pituitary DCE-MRI protocol includes slightly short baseline volume scans compared with other DCE-MRI protocols, however, the first and final dynamic phases are fully sampled without view sharing in our pituitary DCE-MRI protocol. We considered image quality our pituitary DCE-MRI as enough for evaluation, however, the addition of more baseline volume scan may lead to improvement of image quality in DCE-MRI.

In conclusion, IT-TWIST provided better visualization of the posterior lobe, pituitary stalk, neighboring cerebral white matter, and pituitary mass lesions compared with TWIST on 3D pituitary DCE-MRI. In addition, IT-TWIST provided a higher enhancement slope in the posterior lobe and cavernous sinus, with reduced temporal SD in the CSF, sinus air, and corpus callosum compared with TWIST on 3D pituitary DCE-MRI.

Acknowledgements

This work was supported by JSPS KAKENHI Grant Number JP18K07711.

We are grateful to Dr. Aurelien Stalder, Dr. Christoph Forman, and Dr. Michaela Schmidt, for their contribution to IT-TWIST. We are grateful to Mr. Katsutoshi Murata and Mr. Yuta Urushibata, Siemens Healthcare K. K., for protocol optimization.

References

1. STANFIELD JP. The blood supply of the human pituitary gland. J Anat 1960;94:257-273.
2. Leclercq TA, Grisoli F. Arterial blood supply of the normal human pituitary gland. An anatomical study. J Neurosurg 1983;58:678-681.
3. Miki Y, Matsuo M, Nishizawa S, et al. Pituitary adenomas and normal pituitary tissue: enhancement patterns on gadopentetate-enhanced MR imaging. Radiology 1990;177:35-38.
4. Bartynski WS, Lin L. Dynamic and conventional spin-echo MR of pituitary microlesions. AJNR Am J Neuroradiol 1997;18:965-972.
5. Sato N, Sze G, Endo K. Hypophysitis: endocrinologic and dynamic MR findings. AJNR Am J Neuroradiol 1998;19:439-444.
6. Shigematsu Y, Korogi Y, Kitajima M, et al. Abnormal perfusion of the pituitary gland secondary to dural arteriovenous fistulas in the cavernous sinus: dynamic MR findings. AJNR Am J Neuroradiol 2003;24:930-936.
7. Haque TL, Miki Y, Kashii S, et al. Dynamic MR imaging in Tolosa-Hunt syndrome. Eur J Radiol 2004;51:209-217.
8. Suzuki M, Matsui O, Ueda F, et al. Dynamic MR imaging for diagnosis of lesions adjacent to pituitary gland. Eur J Radiol 2005;53:159-167.
9. Takahashi T, Miki Y, Takahashi JA, et al. Ectopic posterior pituitary high signal in preoperative and postoperative macroadenomas: dynamic MR imaging. Eur J Radiol. Volume 55. Ireland; 2005. p. 84-91.
10. Kasaliwal R, Sankhe SS, Lila AR, et al. Volume interpolated 3D-spoiled gradient echo sequence is better than dynamic contrast spin echo sequence for MRI detection of corticotropin secreting pituitary microadenomas. Clin Endocrinol (Oxf) 2013;78:825-830.
11. Fushimi Y, Okada T, Kanagaki M, et al. 3D dynamic pituitary MR imaging with CAIPIRINHA: initial experience and comparison with 2D dynamic MR imaging. Eur J Radiol 2014;83:1900-1906.
12. Rossi Espagnet MC, Bangiyev L, Haber M, et al. High-Resolution DCE-MRI of the Pituitary Gland Using Radial k-Space Acquisition with Compressed Sensing Reconstruction. AJNR Am J Neuroradiol 2015;36:1444-1449.
13. Sen R, Sen C, Pack J, et al. Role of High-Resolution Dynamic Contrast-Enhanced MRI with Golden-Angle Radial Sparse Parallel Reconstruction to Identify the Normal Pituitary Gland in Patients with Macroadenomas. AJNR Am J Neuroradiol 2017;38:1117-1121.
14. Lim RP, Shapiro M, Wang EY, et al. 3D time-resolved MR angiography (MRA) of the carotid arteries with time-resolved imaging with stochastic trajectories: comparison with 3D contrast-enhanced Bolus-Chase MRA and 3D time-of-flight MRA. AJNR Am J Neuroradiol 2008;29:1847-

1854.

15. Winterer JT, Blanke P, Schaefer A, Pache G, Langer M, Markl M. Bilateral contrast-enhanced MR angiography of the hand: diagnostic image quality of accelerated MRI using echo sharing with interleaved stochastic trajectories (TWIST). Eur Radiol 2011;21:1026-1033.
16. Vogt FM, Theysohn JM, Michna D, et al. Contrast-enhanced time-resolved 4D MRA of congenital heart and vessel anomalies: image quality and diagnostic value compared with 3D MRA. Eur Radiol 2013;23:2392-2404.
17. Attenberger UI, Haneder S, Morelli JN, Diehl SJ, Schoenberg SO, Michaely HJ. Peripheral arterial occlusive disease: evaluation of a high spatial and temporal resolution 3-T MR protocol with a low total dose of gadolinium versus conventional angiography. Radiology 2010;257:879-887.
18. Tudorica LA, Oh KY, Roy N, et al. A feasible high spatiotemporal resolution breast DCE-MRI protocol for clinical settings. Magn Reson Imaging 2012;30:1257-1267.
19. Kasel-Seibert M, Lehmann T, Aschenbach R, et al. Assessment of PI-RADS v2 for the Detection of Prostate Cancer. Eur J Radiol 2016;85:726-731.
20. Wetzl J, Forman C, Wintersperger BJ, et al. High-resolution dynamic CE-MRA of the thorax enabled by iterative TWIST reconstruction. Magn Reson Med 2017;77:833-840.
21. Stalder AF, Schmidt M, Quick HH, et al. Highly undersampled contrast-enhanced MRA with iterative reconstruction: Integration in a clinical setting. Magn Reson Med 2015;74:1652-1660.
22. Miki Y, Asato R, Okumura R, Hua F, Konishi J. Contrast enhanced area of posterior pituitary gland in early dynamic MRI exceeds hyperintense area on T1-weighted images. J Comput Assist Tomogr 1992;16:845-848.
23. Piotin M, Tampieri D, Rüfenacht DA, et al. The various MRI patterns of pituitary apoplexy. Eur Radiol 1999;9:918-923.
24. Hayashi Y, Tachibana O, Muramatsu N, et al. Rathke cleft cyst: MR and biomedical analysis of cyst content. J Comput Assist Tomogr 1999;23:34-38.
25. Korogi Y, Takahashi M, Sakamoto Y, Shinzato J. Cavernous sinus: correlation between anatomic and dynamic gadolinium-enhanced MR imaging findings. Radiology 1991;180:235-237.
26. Mahalingam HV, Mani SE, Patel B, et al. Imaging Spectrum of Cavernous Sinus Lesions with Histopathologic Correlation. Radiographics 2019;39:795-819.
27. Rapacchi S, Natsuaki Y, Plotnik A, et al. Reducing view-sharing using compressed sensing in time-resolved contrast-enhanced magnetic resonance angiography. Magnetic resonance in medicine 2015;74:474-481.

Table Legends

Table 1. Demographic details of disease.

Disease	
Macroadenoma	22 (7)
Microadenoma	6 (3)
Hypophysitis	4
Rathke's cleft cyst	3
Stalk transection	1
Normal	15
Total	51

Parenthesis indicates the number of postoperative patients.

Table 2. Results of ROI analyses for enhancement slope.

	TWIST	IT-TWIST	
	Enhancement slope	Enhancement slope	P value
Posterior lobe	12.49 ± 5.05	14.04 ± 5.05	< 0.001
Pituitary stalk	12.14 ± 4.47	13.11 ± 4.43	0.044
Right CS	13.14 (6.96–21.17)*	15.90 (9.80–24.94)*	< 0.001
Left CS	16.40 (10.07–20.96)*	18.03 (11.25–25.22)*	< 0.001

Mean values of enhancement slope with SD are shown. Note that asterisks indicate medians and quartiles. CS = cavernous sinus.

Table 3. Results of ROI analyses for Temporal SD.

	TWIST	IT-TWIST	
	Temporal SD	Temporal SD	P value
Parasellar CSF	8.61 (7.41–10.44)*	5.41 (4.63–6.88)*	< 0.001
Ventricular CSF	6.55 (5.43–7.86)*	2.92 (2.31–4.15)*	< 0.001
Sinus air	5.07 (4.22–5.91)*	3.26 (2.42–4.40)*	< 0.001
Corpus callosum	6.60 ± 1.62	3.13 ± 0.90	< 0.001

Mean values of Temporal SD with SD are shown. Note that asterisks indicate medians and quartiles.

Figure Legends

Figure 1.

(a) Two concept regions of k-space: the central part (region A) contributes to the overall contrast of the image; and the peripheral part (region B) contributes to the rendering of a fine structure. Region B is further divided into several subsegments (four in this example, subregion B1-B4). Each subsegment consists of a quasi-random sampling pattern, such that each subsegment homogeneously covers area B. (b) Acquisition order of the k-space data in k-space acquisition for TWIST; all data in region A and one segment of data in subregion B are alternately acquired for each phase. Temporal resolution of one phase comprises 1A (duration used for acquiring data for region A) and 1B (duration used for acquiring one segment of data in subregion B). (c) The temporal resolution of both TWIST and IT-TWIST is 1A plus 1B, however, the temporal footprint, which is reflected in image quality, is 3As plus 4Bs for TWIST and 1A plus 1B for IT-TWIST. Region B (4 subregion Bs) is fully sampled for TWIST, whereas data in region B (1 subregion B) are partly (sparsely) sampled for IT-TWIST.

Figure 2.

DCE images and calculated parametric maps of TWIST and IT-TWIST are shown. Pituitary stalk (black arrow) and cavernous sinus (white arrow) shows higher values in enhancement slope for IT-TWIST than TWIST. CSF, sinus air, and parasellar brain parenchyma (dashed circle) show lower values in temporal SD for IT-TWIST than TWIST.

Figure 3.

Reference images for visual evaluations of TWIST and IT-TWIST. A subsequently obtained CE 3D T1-GRE sequence was used as "grade 5". Images for grade 4–1 were artificially created using a Gaussian filter. For the evaluation of delineation of pituitary stalk, posterior lobe during the arterial phase, and delineation of the mass lesion border, normal sagittal images and coronal images of macroadenoma were resampled as 1-mm isotropic voxels and underwent application of a 5-step Gaussian blurring filter (grade 5, no filter; grade 4–1, sigma = 0.4, 0.8, 1.2, and 1.6, respectively). For the evaluation of cerebral white matter around the sella, normal coronal images were resampled as 1-mm isotropic voxels with application of a 5-step Gaussian noise filter (grade 5, no filter; grade 4-1, SD = 2, 4, 6, and 8; grade 5 is the best).

Figure 4.

Scores for visual evaluations of posterior lobe, pituitary stalk, mass lesion and cerebral white matter with TWIST and IT-TWIST. Graph bars indicate median and error bars indicate interquartile range of TWIST and IT-TWIST. All items are evaluated significantly better in IT-TWIST than TWIST. Asterisks indicate statistical significance ($P < 0.0125$).

Figure 5.

(a) Enhancement slope of posterior lobe, pituitary stalk, and bilateral cavernous sinus with TWIST and IT-TWIST. Enhancement slope of posterior lobe and bilateral cavernous sinus is significantly higher with IT-TWIST than with TWIST. (b) Temporal SD of parasellar CSF, ventricular CSF, sinus air and corpus callosum in TWIST and IT-TWIST. All items are significantly lower in IT-TWIST than TWIST. Asterisks indicate statistical significance ($P < 0.00625$).

Figure 6.

A 33-year-old woman with normal pituitary gland. (a) Sagittal images of the 3rd, 4th, 5th and 6th dynamic phase images with TWIST and IT-TWIST. Pituitary stalk (white arrow) and posterior lobe (black arrow) are enhanced from the 4th dynamic phase. Early enhancement of pituitary stalk and posterior lobe are better visualized in IT-TWIST than TWIST. Less noise is visualized in parasellar CSF and sinus air in IT-TWIST than TWIST. * = parasellar CSF; ** = sinus air. (b) Coronal images of the 6th dynamic phase. Less noise is visualized in corpus callosum (white arrowhead) and ventricular CSF (black arrowhead) in IT-TWIST than TWIST.

Figure 7.

A 43-year-old woman with microadenoma. Axial images of the 3rd, 4th, 5th and 15th dynamic phase images in TWIST and IT-TWIST. In both TWIST and IT-TWIST images, posterior lobe (white arrow) is enhanced in the 3rd phase; subsequently microadenoma (black arrow) in right posterior part of pituitary is enhanced in the 4th phase; anterior lobe (white arrowhead) is gradually enhanced in the 5th phase. In IT-TWIST, the boundary of the tumor is more clearly depicted than TWIST in the 15th phase.

Figure 8.

A 47-year-old man with pituitary macroadenoma. Sagittal images of the 1st, 4th, 5th and 6th dynamic phases are shown. Pituitary stalk and posterior lobe are compressed by macroadenoma (*). Posterior lobe hyperintensity (white arrow) in the 1st dynamic phase is visualized in IT-TWIST better than TWIST. In the 4th, 5th and 6th dynamic phases, early enhancement of both pituitary stalk (black arrow) and posterior lobe (white arrow), and border of macroadenoma is more clearly delineated in IT-TWIST than TWIST.

Supplementary figure 1.

A 33-year-old woman with normal pituitary gland shown in the Figure 6. Time-intensity curves of posterior lobe, pituitary stalk, and bilateral cavernous sinus are shown. The slope of enhancement is visually higher in pituitary stalk and right cavernous sinus in IT-TWIST than in TWIST. In TWIST, signal intensity tends to fluctuate comparing IT-TWIST. As for the posterior lobe, the slope of enhancement was slightly higher in TWIST compared with IT-TWIST. We suspected that k-space data (subregion B1-B4) used for creating 2nd dynamic phase in TWIST may increase the signal intensity. Note that dynamic curve was normalized by the 1st phase intensity. Contrast medium injection starts at 10 seconds.

Supplementary figure 2.

A 43-year-old woman with microadenoma shown in the Figure 7. Time-intensity curves of posterior lobe, pituitary stalk, and bilateral cavernous sinus are shown. The slope of enhancement to the peak is visually higher in all ROIs in IT-TWIST than in TWIST. In IT-TWIST, signal intensity gradually decreases. In TWIST, signal intensity tends to fluctuate compared with IT-TWIST, especially in the late dynamic phases. Note that dynamic curve was normalized by the 1st phase intensity. Contrast medium injection starts at 10 seconds.

Supplementary figure 3.

A 47-year-old man with pituitary macroadenoma shown in the Figure 8. Time-intensity curves of posterior lobe, pituitary stalk, and bilateral cavernous sinus are shown. The slope of enhancement to the peak is visually higher in pituitary stalk and bilateral cavernous sinus in IT-TWIST than in TWIST. In TWIST, signal intensity obviously fluctuated compared with IT-TWIST, especially in pituitary lobe and pituitary stalk. Note that dynamic curve was normalized by the 1st phase intensity. This normalization method may affect higher intensity ration of posterior lobe in TWIST compared with IT-

TWIST, however, further evaluation is necessary. Contrast medium injection starts at 10 seconds.

Figure 1.

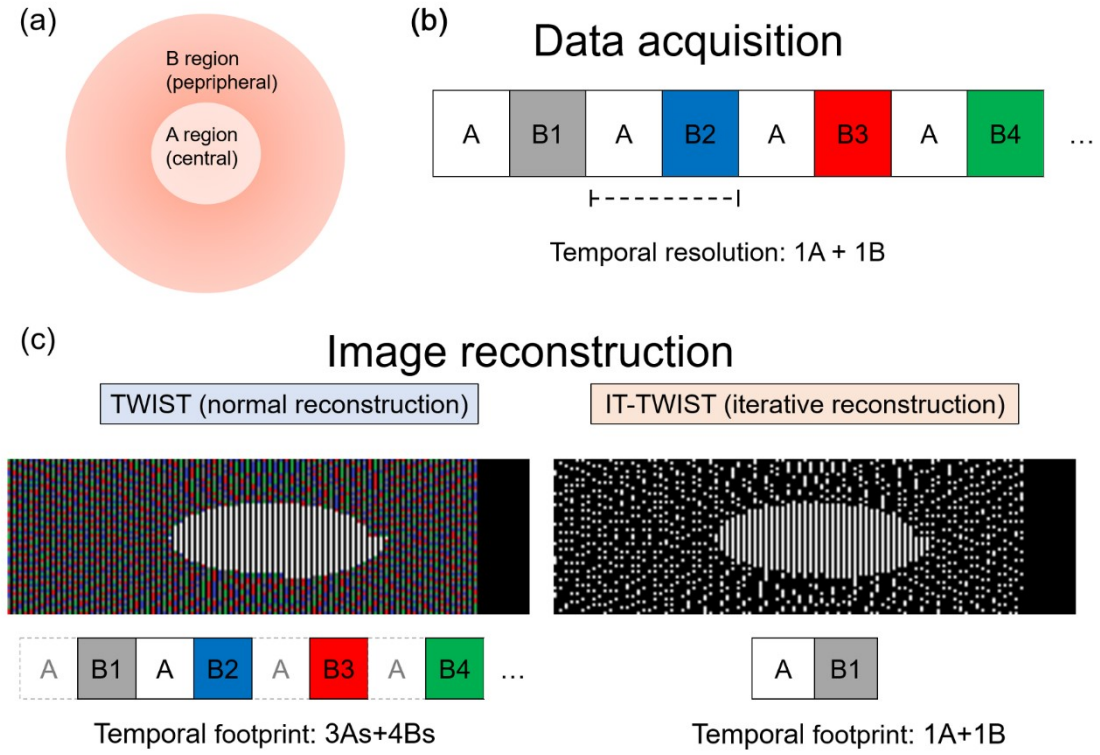
(a)
B region
(pepripheral)
A region
(central)
(b)
Data acquisition
A
B1
A
B2
A
B3
A
B4
…
Temporal resolution: 1A + 1B
(c)
Image reconstruction
TWIST (normal reconstruction)
IT-TWIST (iterative reconstruction)
A
B1
A
B2
A
B3
A
B4
…
A
B1
Temporal footprint: 3As+4Bs
Temporal footprint: 1A+1B

Figure 2.

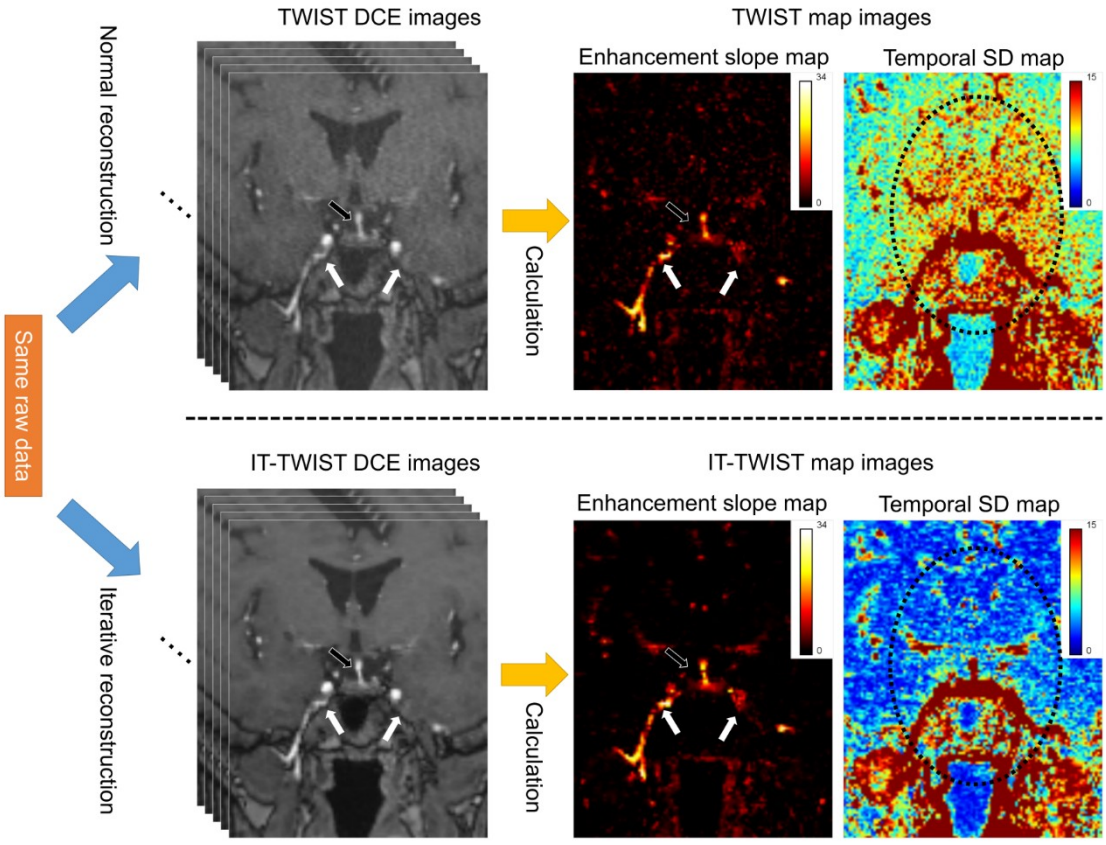
Same raw data
Normal reconstruction
Iterative reconstruction
TWIST DCE images
IT-TWIST DCE images
Calculation
Calculation
TWIST map images
IT-TWIST map images
Enhancement slope map
Temporal SD map
Enhancement slope map
Temporal SD map
34
0
15
0
34
0
15
0

Figure 3.

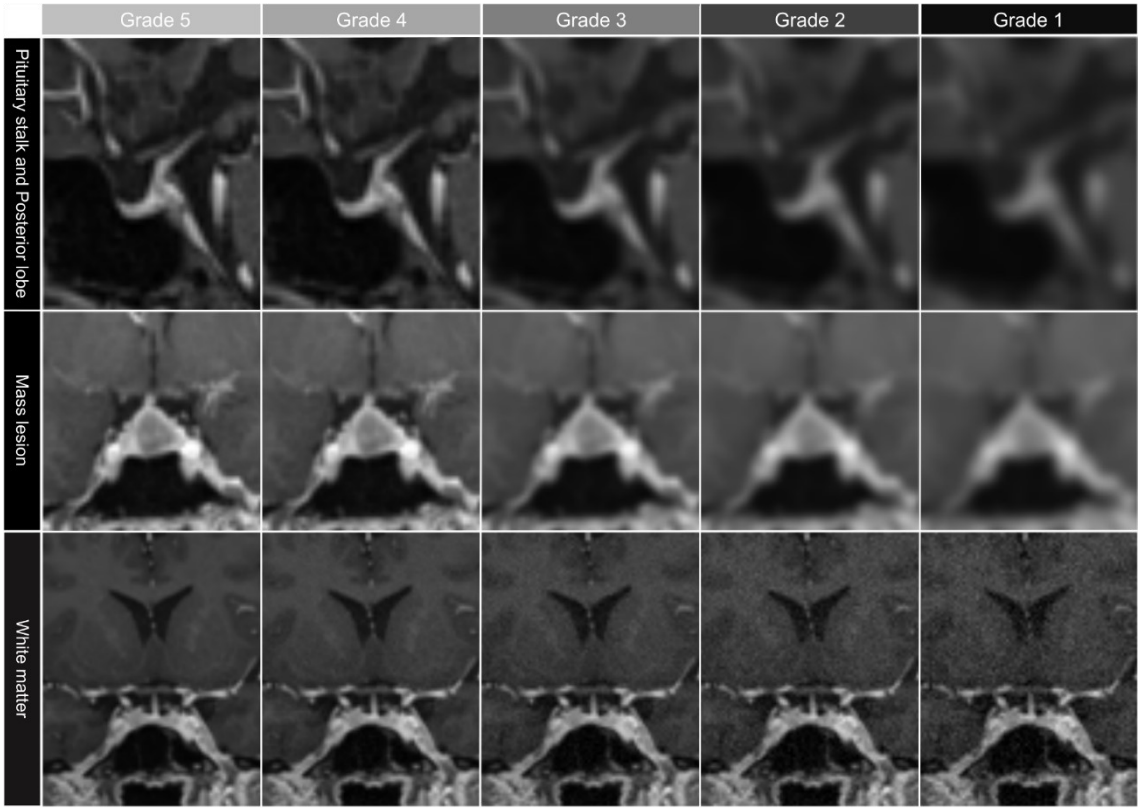
Grade 5
Grade 4
Grade 3
Grade 2
Grade 1
Pituitary stalk and Posterior lobe
Mass lesion
White matter

Figure 4.

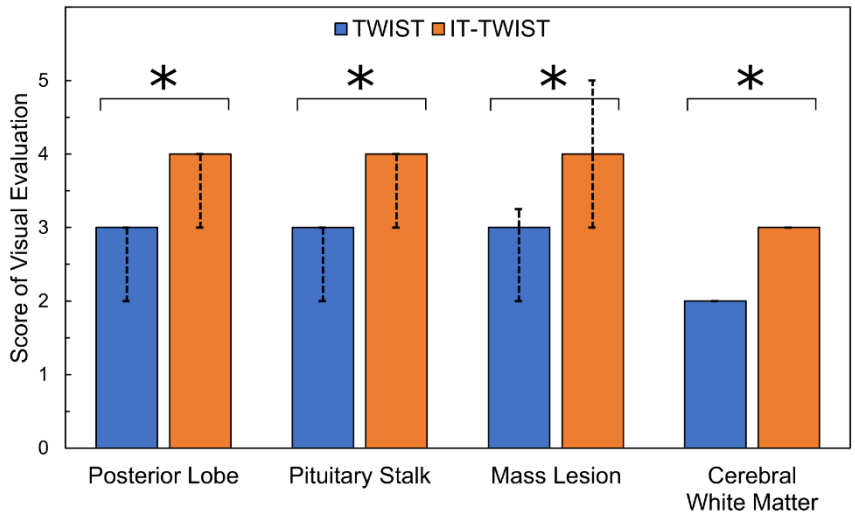
TWIST
IT-TWIST
Score of Visual Evaluation
0
1
2
3
4
5
*
*
*
*
Posterior Lobe
Pituitary Stalk
Mass Lesion
Cerebral White Matter

Figure 5.

(a)

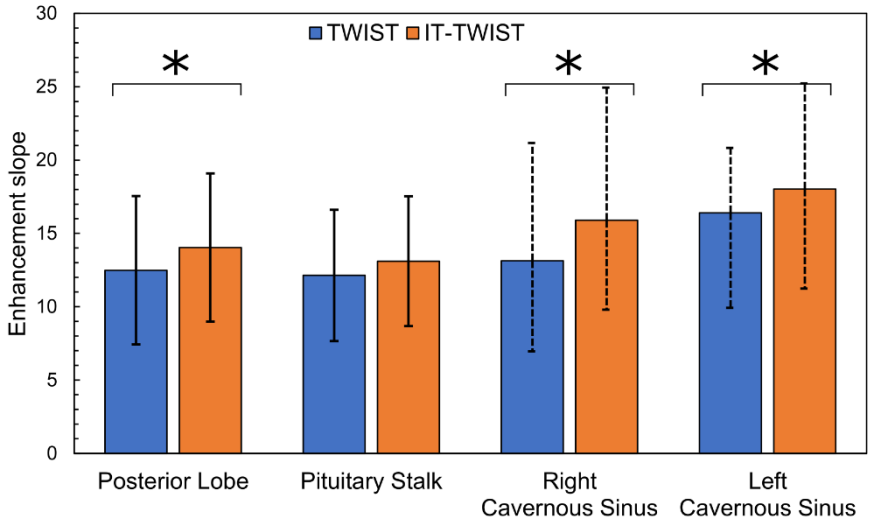
TWIST
IT-TWIST
Enhancement slope
30
25
20
15
10
5
0
*
*
*
Posterior Lobe
Pituitary Stalk
Right Cavernous Sinus
Left Cavernous Sinus

(b)

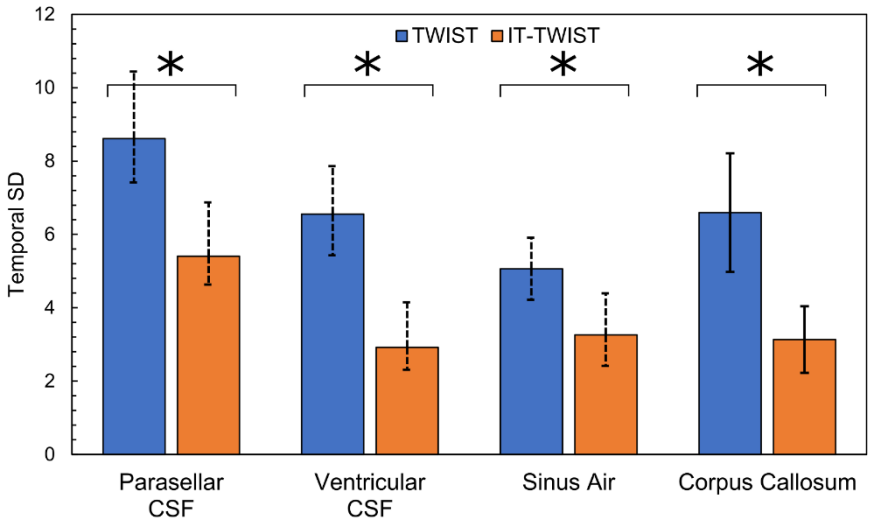
TWIST
IT-TWIST
Temporal SD
12
10
8
6
4
2
0
*
*
*
*
Parasellar CSF
Ventricular CSF
Sinus Air
Corpus Callosum

Figure 6.

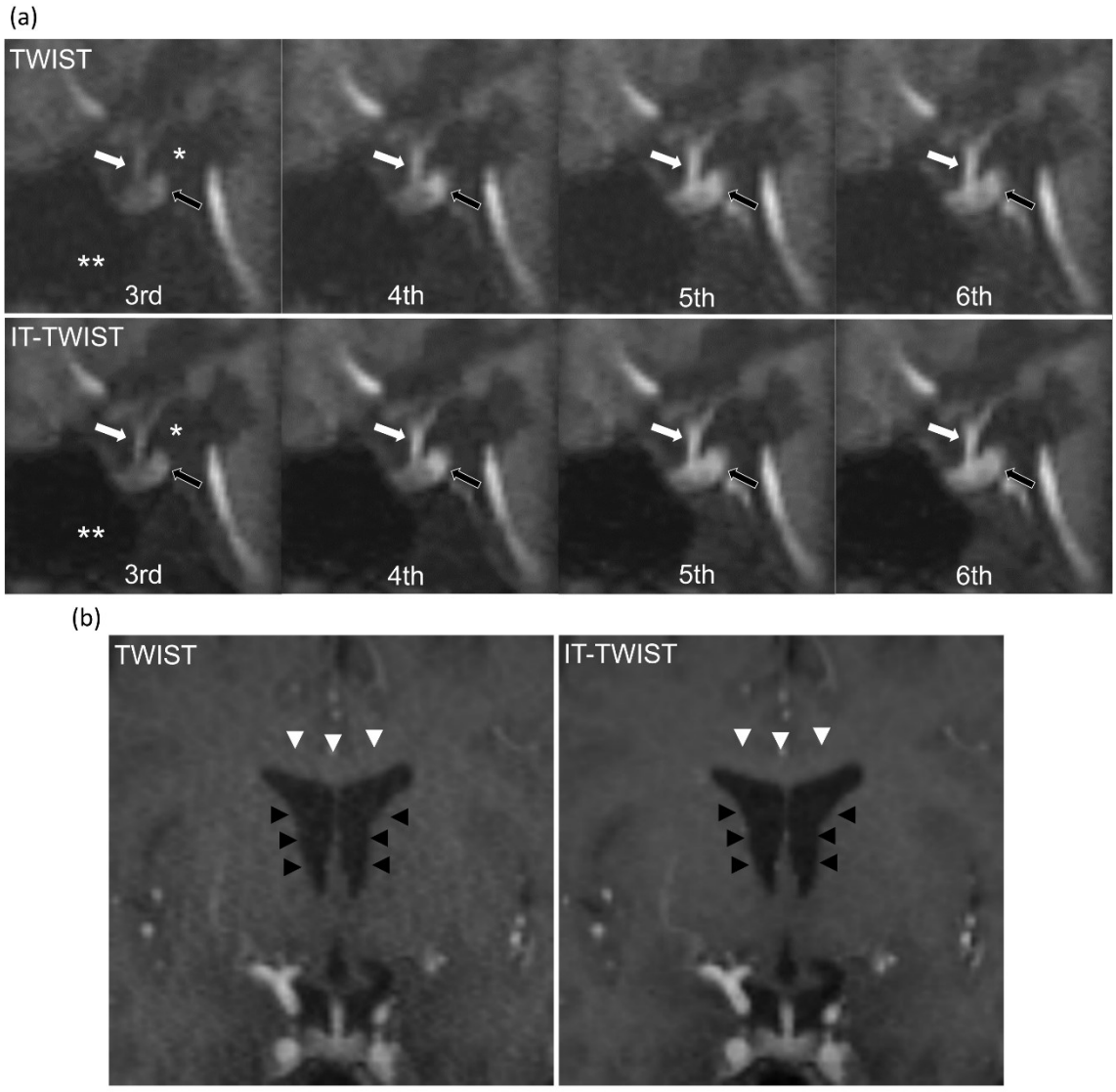
(a)
TWIST
*
**
3rd
4th
5th
6th
IT-TWIST
*
**
3rd
4th
5th
6th
(b)
TWIST
IT-TWIST

Figure 7.

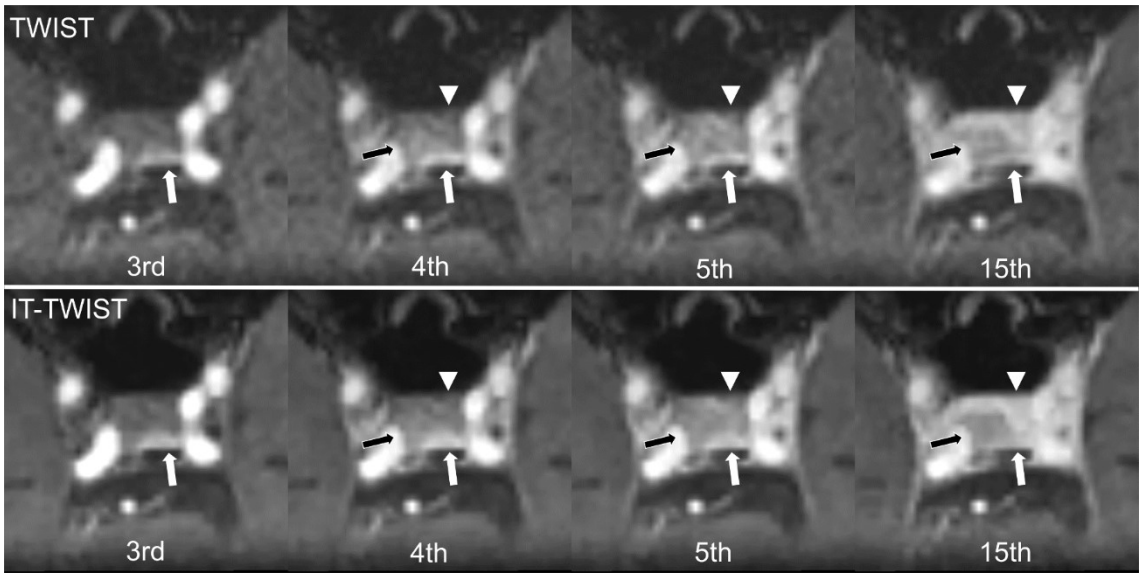

Figure 8.

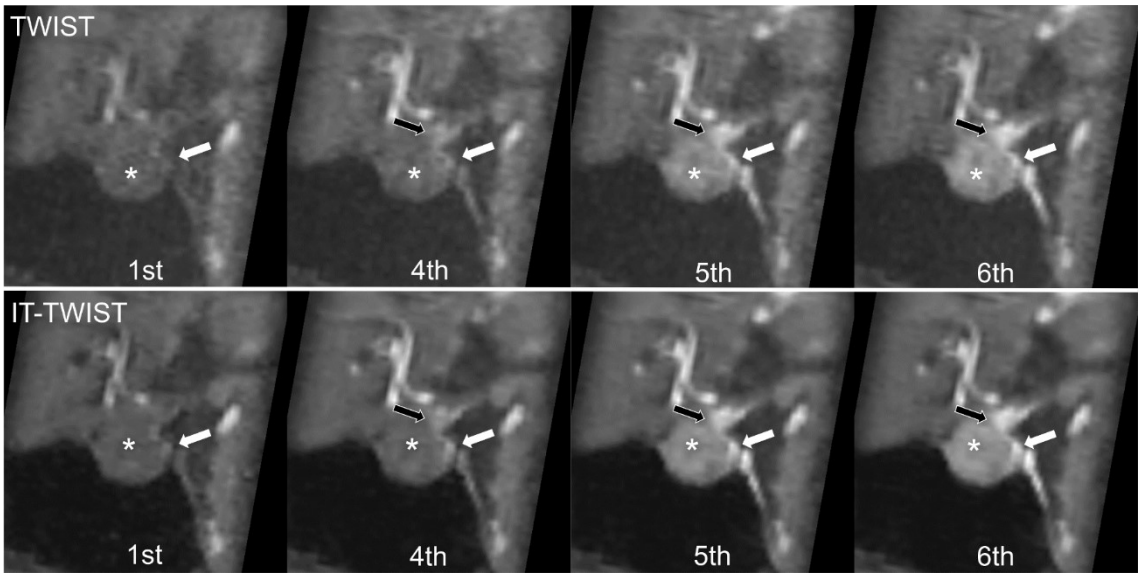

Supplementary figure 1.

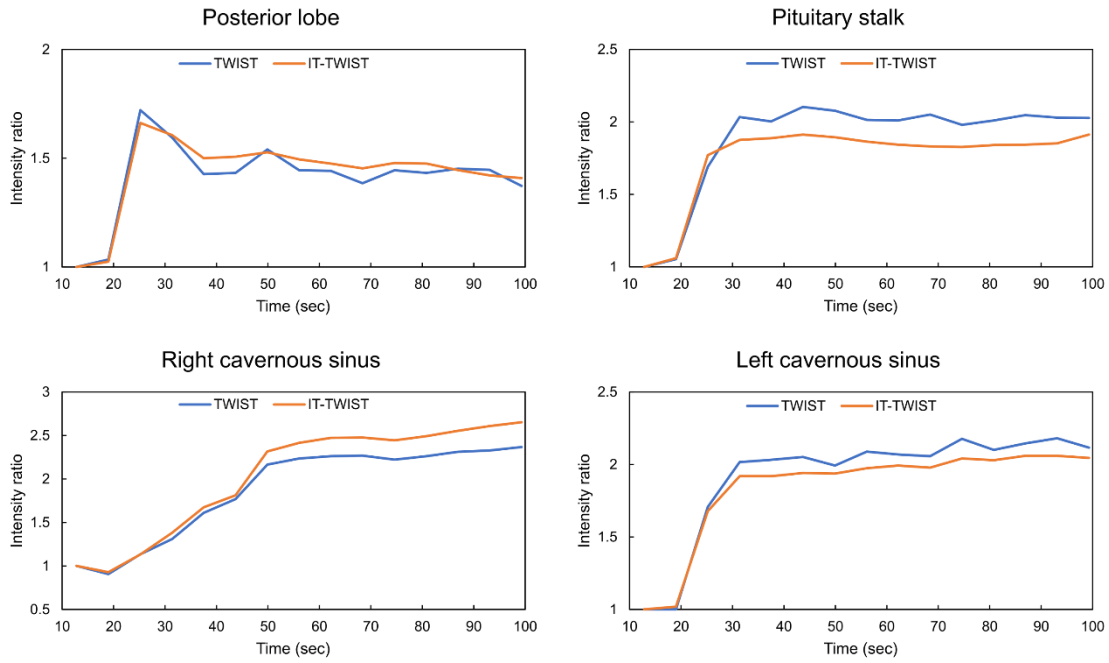

Supplementary figure 2.

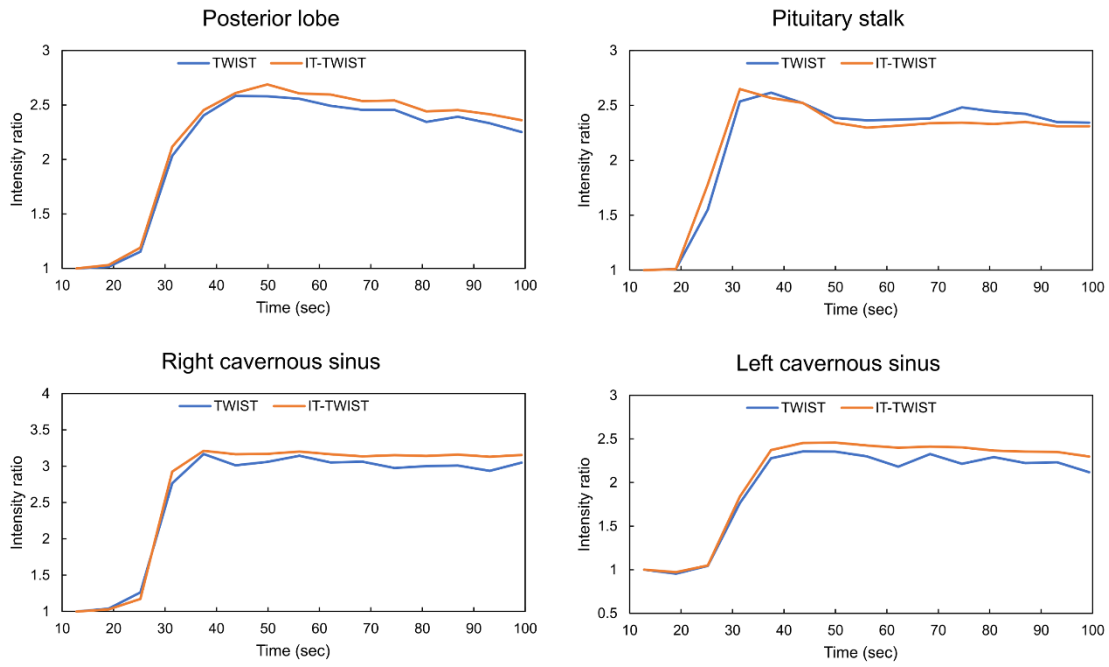

Supplementary figure 3.